Discover Applied Sciences

Research

Forecasting renewable energy for microgrids using machine learning

Piyumi Sudasinghe[1] · Damayanthi Herath[2] · Isiwara Karunarathne[1] · Hansani Weeratunge[3] · Lahiru Jayasuriya[4]

Received: 23 December 2024 / Accepted: 7 April 2025
Published online: 03 May 2025

Abstract
Microgrids, comprised of interconnected loads and distributed energy resources, function as single controllable entities with respect to the main grid. However, the inherent variability of distributed wind and solar generation within microgrids presents operational stability challenges concerning voltage regulation and frequency stability. Accurate forecasting of renewable generation is crucial for mitigating these challenges. This work proposes a one-dimensional Convolutional Neural Network (1-D CNN) based approach to forecast photovoltaic (PV) generation and wind energy, using data from the University of California, San Diego microgrid and San Diego Airport weather records. The proposed method is evaluated against various forecasting methods using key metrics: Mean Squared Error (MSE), Mean Absolute Error (MAE), Root Mean Squared Error (RMSE), and R-squared value. Results show that the 1-D CNN model achieves an improvement of up to 229.8 times in MSE and a 24.47 fold improvement in MAE compared to baseline models that use traditional statistical methods in forecasting. This demonstrates the potential of machine learning for enhancing microgrid management, particularly in short-term forecasting of renewable generation.

Article Highlights

- Evaluated ML-based renewable energy forecasting models by implementing 1-D CNN and LSTM models using real-world data.
- Proposed 1-D CNN performs better than LSTM and baseline models, achieving higher accuracy and computational efficiency.
- Accurate forecasting of PV and wind energy generation enhances grid stability, reduces backup power dependency, and supports sustainable energy integration.

Keywords Machine learning · Renewable energy forecasting · PV energy · Wind speed · Microgrid · 1-D CNN

Supplementary Information The online version contains supplementary material available at https://doi.org/10.1007/s42452-025-06895-5.

✉ Piyumi Sudasinghe, piyumi.sudasinghe@eng.pdn.ac.lk; ✉ Damayanthi Herath, damayanthiherath@eng.pdn.ac.lk; Isiwara Karunarathne, isiwarakaru@gmail.com; Hansani Weeratunge, hansani.w@sliit.lk; Lahiru Jayasuriya, ltjayasu@tec.rjt.ac.lk | [1]Department of Mechanical Engineering, University of Peradeniya, Peradeniya, Sri Lanka. [2]Department of Computer Engineering, University of Peradeniya, Peradeniya, Sri Lanka. [3]Department of Mechanical Engineering, Sri Lanka Institute of Information Technology, Malabe, Sri Lanka. [4]Department of Electrical and Electronic Technology, Faculty of Technology, Rajarata University of Sri Lanka, Mihintale, Sri Lanka.

1 Introduction

A microgrid is a localized group of electricity sources and loads that can operate independently or in conjunction with the main grid [1, 2]. It typically consists of distributed energy resources (DERs) such as renewable energy sources (solar, wind), energy storage systems, and backup generators, along with controllable loads. These components are integrated into a single system that can generate, distribute, and manage electricity within a specific location, such as a campus, community, industrial complex, or military base [2–4].

PV and wind energy are two of the most widely used renewable energy sources. The integration of these energy sources into power systems, including microgrids, is essential for reducing greenhouse gas emissions and mitigating the impacts of climate change [5, 6]. However, the integration of renewable energy sources into power systems in general presents several challenges [1, 7]. One of the main challenges is the variable nature of renewable energy generation, which can cause fluctuations in power supply and affect the stability of the grid [1, 3, 8]. To address this challenge, accurate forecasting of renewable energy generation is essential for effective planning and operation of power systems [4, 9].

1.1 Machine learning in forecasting renewable energy generation

In recent years, there has been growing interest in the application of machine learning techniques for improving the accuracy of renewable energy generation forecasting. Machine learning models, such as artificial neural networks, support vector machines, and decision trees, have been used to model the complex relationships between weather variables and renewable energy generation [10, 11]. These models utilize historical data to make accurate predictions of future renewable energy generation [1, 3]. In this study, we focus on PV energy generation and wind availability forecasting, which are widely adopted renewable sources.

Since PV and wind energy generation are affected by a range of weather variables, such as solar irradiance, wind speed, and air temperature, traditional forecasting methods, such as time series analysis and numerical weather prediction models, have limitations in their ability to accurately capture the complex relationships between weather variables and renewable energy generation [1, 12, 13]. These include oversimplified assumptions [14], handling high-dimensional data [15], inadequate temporal resolution [16], lack of probabilistic information [17], and difficulty adapting to new patterns [18]. As a result, there is a need for more effective forecasting techniques that can improve the accuracy of PV and wind energy generation forecasting [1, 19] such as, machine learning and deep learning.

Machine learning techniques have emerged as effective tools for enhancing the accuracy of PV and wind energy generation forecasting, with models such as artificial neural networks, support vector machines, and decision trees showing significant promise [11]. They have demonstrated the potential of machine learning techniques to accurately model the complex relationships between weather variables and renewable energy generation [1, 3].

For example, Artificial Neural Networks (ANNs) have been utilized to predict solar energy generation using weather forecasts, demonstrating accurate forecasting capabilities and supporting the integration of renewable energy sources into power systems [20]. Forecasting energy generation allows for better alignment of energy supply with demand, leading to cost reductions by minimizing the use of expensive backup power and enhancing grid stability by enabling better management of energy fluctuations, ensuring a continuous and reliable power supply [11, 20, 21]. Additionally, accurate predictions of Energy generation support demand response strategies, contributing to a more flexible and efficient energy system, and facilitating the integration of renewable energy sources [1, 3, 20].

Long short-term memory (LSTM) recurrent neural networks have also been deployed to forecast day-ahead solar irradiance availability for electricity generation in microgrids, achieving significant improvements in forecasting accuracy compared to traditional methods like autoregressive integrated moving average (ARIMA) and seasonal ARIMA (SARIMA) [21, 22]. Therefore, existing literature suggests that the Neural Networks can recognize variability and patterns in weather variables like solar irradiance significantly [23]. Solar irradiance directly influences the amount of energy produced by PV panels. Precise solar irradiance forecasts using Neural Networks show their ability to model complex, nonlinear relationships in data making them well-suited for this task. By learning patterns from historical solar irradiance and weather data, neural networks can provide more accurate and reliable renewable energy forecasts.

In addition to improving forecasting accuracy, machine learning techniques have the ability to provide valuable insights into the factors that affect renewable energy generation. For example, Machine learning models such as

ANNs, support vector machines (SVM), and decision trees (DT) have been able to estimate renewable energy potential based on climatic and weather data [6]. These algorithms could identify important relationships between weather variables and renewable energy generation. For instance, higher temperatures and lower humidity levels were linked to increased solar energy generation, while higher wind speeds boosted wind energy generation [1, 6].

Neural Networks have shown better results than traditional methods in predicting and forecasting weather variables, and the existing literature suggests that Neural Networks have significant potential to improve the accuracy of PV and wind energy forecasting [1, 3, 5, 6, 9–11, 17–21, 24]. Further research is needed to develop and evaluate advanced machine learning algorithms for PV and wind energy forecasting [1, 25]. Deep learning models, such as CNNs, LSTM networks and Gated Recurrent Units (GRUs) are commonly applied in time-series forecasting [26, 27]. Recurrent models like LSTMs and GRUs are designed to capture long-term dependencies using memory cells, but they often face high computational costs and sequential processing limitations, leading to slower training and inference times [28–30]. In contrast, 1D CNNs use convolutional filters to efficiently capture local temporal dependencies [31], enabling parallelized computation and faster processing [32], making them particularly suitable for real-time applications and large-scale datasets [33–36]. Traditional statistical models such as ARIMA and Exponential Smoothing (ETS), also struggle to capture the complex, nonlinear patterns found in renewable energy data, which often exhibit high variability and non-stationarity [37–39]. Several studies have demonstrated that CNN-based architectures has shown better forecasting accuracy compared to both recurrent models and conventional statistical approaches [40], while maintaining lower computational complexity [35]. The motivation for using 1D CNNs lies in their ability to efficiently extract spatiotemporal features, resulting in faster training and inference times [35, 40–43]. Recent research has also highlighted the potential of 1D CNNs in renewable energy forecasting, particularly for applications such as photovoltaic (PV) generation and wind speed prediction, where local temporal patterns play a critical role [1, 41, 44]. Building on these findings, this study aims to evaluate the effectiveness of 1D CNNs for renewable energy forecasting in microgrid applications, contributing to the growing body of research on efficient and accurate forecasting methods for renewable energy systems.

2 Methodology

2.1 Data collection and preparation

Accurate forecasting for microgrids depends on the quality of the data collected, which must be accurate, complete, well-documented, continuous, and carefully prepared. This approach ensures the precision of forecasts and supports the overall research process, making the results reliable and reproducible.

2.1.1 PV generation data

The primary data sources of this research consist of two open-source datasets. The first dataset used in this research comes from historical PV generation data found in an open-source multi-year dataset by Silwal [4]. This is a public comprehensive dataset covering different parts of the University of California, San Diego microgrids power generation, loads, etc. This microgrid integrates various DERs such as solar power plants, electric vehicles, buildings, a gas-fired combined heat and power plant, and electric and thermal energy storage systems. Most datasets in this collection provide 15-minute averages of real and reactive power spanning from January 21, 2015, to February 29, 2020. AS the primary input, this dataset provides valuable insights into the variability of PV generation within a microgrid context because, this dataset includes multiple PV systems covering different locations of the University of California, within the same microgrid, capturing a wider area.

Table 1 shows the Metadata of the released data of on-campus Solar PV Generators data [4]. From this comprehensive dataset, a selection process was undertaken to choose 10 PV generation datasets. Key factors, including the starting date, end date, and the number of missing days, were considered during this selection. This careful consideration ensures that by incorporating information on starting and ending dates, along with minimizing missing data, the selected PV generation datasets form a representative and reliable dataset for further analysis and model development.

In Table 2, missing data is represented as missing days. Considering a 15-min interval, one missing day corresponds to 24*4 which is 96 data points. The selected data exhibits relatively low missing values. Notably, while the End Date remains consistent, variations in the Starting Date are observed among the selected different PV generators.

Table 1 On-campus solar PV generators data (Unk-unknown, NA-not applicable)

Facility	PV rating				
	(DC, AC kW)	Data file name	Start date	End date	Missing days
F1	Unk, 390	Bsb_libraryPV.csv	21 Jan, 2015	29 Feb, 2020	0.5
F2	284, Unk	bsb_buildingPV.csv	21 Jan, 2015	30 Aug, 2018	0.2
F3	Unk, 74	BioengineeringPV.csv	21 Jan, 2015	29 Feb, 2020	26.7
F4	Unk, 54	Csc_buildingPV.csv	15 Jan, 2016	29 Feb, 2020	49.4
F5	Unk, 65	Cup_PV.csv	01 Jan, 2015	29 Feb, 2020	0.4
F6	43, 35	Ebu2_a_PV.csv	27 April, 2015	29 Feb, 2020	0.3
F7	37, 31	Ebu2_b_PV.csv	27 April, 2015	29 Feb, 2020	0.3
F8	Unk, Unk	Electricshop_PV.csv	24 Oct, 2015	29 Feb, 2020	0.2
F9	29, 24	Garagefleets_PV.csv	18 Mar, 2016	29 Feb, 2020	0.4
F10	195, 200	GilmanparkingPV.csv	09 May, 2015	29 Feb, 2020	812.1
F11	338, 350	HopkinsparkingPV.csv	29 Aug, 2015	29 Feb, 2020	1
F12	41, Unk	Keelinga_PV.csv	15 May, 2017	29 Feb, 2020	0.1
F13	Unk, Unk	Keelingb_PV.csv	15 May, 2017	29 Feb, 2020	0.1
F14	18, Unk	KyoceraskylinePV.csv	14 Feb, 2016	29 Feb, 2020	200.7
F15	Unk, 50	LeichtagPV.csv	01 Jan, 2015	29 Feb, 2020	0.3
F16	61, Unk	Mesom_PV.csv	31 Mar, 2016	29 Feb, 2020	14.3
F17	Unk, 120	MayerhallPV.csv	01 Jan, 2015	29 Feb, 2020	0.4
F18	268, Unk	OslerparkingPV.csv	17 Dec, 2018	29 Feb, 2020	185.4
F19	63, 75	Pricecenter_a_PV.csv	27 April, 2015	29 Feb, 2020	0.3
F20	66, 75	Pricecenter_b_PV.csv	23 May, 2015	29 Feb, 2020	0.2
F21	Unk, 65	Sdsc_PV.csv	01 Jan, 2015	29 Feb, 2020	0.3
F22	Unk, 120	Sme_solarPV.csv	14 Oct, 2016	29 Feb, 2020	0.1
F23	6.5, Unk	PowellPV.csv	01 Jan, 2015	03 Mar, 2016	0.1
F24	49, Unk	Stephenbirch_PV.csv	12 April, 2016	29 Feb, 2020	0.1

The facilities associated with the on-campus solar PV generators are as follows: Biomedical Sciences Library (F1), Biomedical Sciences Building (F2), Bio-Engineering Hall (F3), Campus Services Complex (F4), Central Utility Plant (F5), Engineering Building Unit II (F6), Engineering Building Unit II (F7, duplicate entry), Electric Shop (F8), Fleet Services (F9), Gilman Parking (F10), Hopkins Parking (F11), Keeling Apartments (F12), Keeling Apartments (F13, duplicate entry), Otterson Hall (F14), Leichtag Biomedical Research (F15), MESOM Laboratory (F16), Mayer Hall (F17), Osler Parking (F18), Price Center (F19), Price Center (F20, duplicate entry), San Diego Supercomputing Center (F21), Structural and Material Engineering (F22), Powell Structural Research Lab (F23), and Birch Aquarium (F24). [4]

Table 2 Selected on-campus solar PV generators data for the forecasting of PV energy (Unk-unknown) [4]

PV generator	Facility	Start date	End date	Missing days
PV1	F1	21 Jan, 2015	29 Feb, 2020	0.5
PV2	F5	01 Jan, 2015	29 Feb, 2020	0.4
PV3	F6	27 April, 2015	29 Feb, 2020	0.3
PV4	F7	27 April, 2015	29 Feb, 2020	0.3
PV5	F8	24 Oct, 2015	29 Feb, 2020	0.2
PV6	F9	18 Mar, 2016	29 Feb, 2020	0.4
PV7	F11	29 Aug, 2015	29 Feb, 2020	1
PV8	F17	01 Jan, 2015	29 Feb, 2020	0.4
PV9	F21	01 Jan, 2015	29 Feb, 2020	0.3
PV10	F24	12 April, 2016	29 Feb, 2020	0.1

2.1.2 Weather data

The second data set is from Historical weather and climate data from the San Diego International Airport, CA, US [15]. Hourly weather data from January 21, 2015, to February 29, 2020, has been considered for analysis. This timeframe corresponds with the selected PV generation data range, allowing for an examination of the weather conditions and their impact on photovoltaic energy production.

The Meteostat API uses abbreviations to describe meteorological parameters and the units of the parameters are shown in Table 3. These will be the units of the weather data considered in this work.

2.1.3 Considering hourly data

Hourly data is commonly used in forecasting because it provides a clearer and more organized view of trends. This study also uses hourly data, as it helps improve forecasting accuracy by reducing short-term fluctuations or "noise" in the data. It simplifies analysis by highlighting important patterns in energy generation without becoming overwhelmed by excessive detail. Overall, using hourly data makes the forecasting process more efficient and effective.

A conversion process is applied to the PV data to align its time granularity with the selected weather data. The PV data, originally recorded in 15-min intervals, is converted to hourly data by calculating the mean of every four consecutive 15-min data points. Averaging the shorter intervals helps reduce noise and better capture overall trends [45]. This adjustment aligns the timing of both datasets, making it easier to analyze the connection between hourly weather conditions and photovoltaic energy generation. The equation for converting 15-minute interval PV data to hourly data by calculating the mean of every four consecutive 15-minute data points can be expressed as follows

$$\text{Hourly PV Data} = \frac{\text{PV Data}_t + \text{PV Data}_{t+1} + \text{PV Data}_{t+2} + \text{PV Data}_{t+3}}{4}. \quad (1)$$

Hourly PV Generation is the average PV generation for the hour starting at data point t and $t+1$, $t+2$, and $t+3$ represent the subsequent 15-min intervals within the same hour. $PVData_t$ is the instantaneous PV generation data in kW at data point t (15-min interval data).

2.2 Data analysis

This study undergoes several data preprocessing and feature engineering steps. The steps include cleaning the data for analysis by filling in missing data, removing outliers, and normalizing and scaling the data. Furthermore, Feature engineering steps include selecting relevant features and transforming them into a format. This includes creating

Table 3 Meteorological parameters and units from San Diego airport dataset

Code	Meaning	Unit
TEMP	Air temperature	°C
TAVG	Average temperature	°C
TMIN	Minimum temperature	°C
TMAX	Maximum temperature	°C
DWPT	Dew point	°C
PRCP	Total precipitation	mm
WDIR	Wind (from) direction	Degrees
WSPD	Average wind speed	km/h
WPGT	Wind peak gust	km/h
RHUM	Relative humidity	%
PRES	Sea-level air pressure	hPa
SNOW	Snow depth	mm
TSUN	Total sunshine duration	Minutes
COCO	Weather condition code	–

interaction terms and applying mathematical transformations to the data. All these steps are important in obtaining a better dataset for the forecasting purpose.

2.2.1 Exploratory data analysis (EDA) on datasets

A Pandas profiling analysis was conducted to generate a detailed report of the PV generation dataset. The data was first organized by date and time, and duplicate entries were removed to ensure accuracy. The 10 PV generation datasets were then merged into a single dataset for further analysis. However, the varying starting dates posed a challenge, leading to missing values at the initial timestamps. Addressing these missing values required handling two distinct issues: actual data gaps and differences arising from the varying starting dates. These were managed using appropriate techniques based on the data analysis results.

Similarly, an initial EDA was performed on the weather dataset, supported by a Pandas profiling analysis and a heatmap correlation plot for feature selection. After selecting the relevant features, the weather dataset was organized by sorting entries according to the *datetime* column. Duplicate entries were identified and removed to maintain data integrity, ensuring that only unique timestamps were retained.

2.3 Data preprocessing and feature engineering

Based on the results obtained from the EDA for both datasets, additional data preprocessing and feature engineering techniques were applied. These included removing outliers, handling missing values, and selecting relevant features to create the input data for the forecasting models.

The preprocessed PV generation dataset was resampled by averaging four consecutive data points into 15-min intervals, resulting in a smoother and more manageable hourly dataset for analysis.

The final preprocessed two datasets were used in the forecasting of PV energy generation and wind speed as described in the next sections.

2.3.1 Data splitting

The datasets selected for the forecasting model inputs were divided into three parts: training, validation, and test sets, with a distribution of (70%, 20%, 10%), respectively. This split allows the model to learn from the majority of the data during training, validate its performance on a separate portion, and finally, test its capabilities on an unseen data set.

2.3.2 Wind speed forecasting data

For wind speed forecasting, the preprocessed weather dataset was considered. The dataset was normalized using the standardization method and then splitted. Z-score normalization, also known as standardization, adjusts the data to have a mean of 0 and a standard deviation of 1, ensuring that each feature contributes equally to the model, irrespective of its original scale or distribution. Data normalization using standardization technique enhances model performance by ensuring that input features are on a comparable scale and distribution, and is particularly advantageous due to its robustness to outliers. It's important to note that the mean and standard deviation for this normalization followed in this study were computed exclusively using the training data. It ensures that the models are unaware of the values in the validation and test sets, maintaining the integrity of the training process.

2.3.3 PV generation forecasting data

For PV generation forecasting, the preprocessed weather dataset is merged with the normalized PV generation data based on the timestamp. By integration of datasets, the model gains valuable insights into the dependencies and correlations between weather conditions and PV energy production, enhancing the accuracy and effectiveness of the forecasting model. After merging a specific start time for the dataset has been decided considering PV generation data which is *2016-01-01 00:00:00*.

For the PV generation forecasting, the *wspd* feature has been removed since *wspd* is not the target variable and the information related to wind speed is already incorporated within the *wind vector* feature. Removing redundant

Table 4 Model inputs/outputs summary table

Category	Feature	Description
Inputs	Temperature	Air temperature in °C, affecting solar irradiance.
	Dew point	Measure of atmospheric moisture.
	Relative humidity	Percentage of humidity
	Wind speed	Average wind speed in km/h
	Sea-level air pressure	Atmospheric pressure in hPa
	Wind vector components	Derived from wind speed and direction
	Day sine and cosine signals	Temporal features capturing daily periodicity.
	Year sine and cosine signals	Temporal features capturing annual periodicity.
Outputs	PV energy generation	Forecasted photovoltaic power output.
	Wind speed	Forecasted wind speed for energy generation.

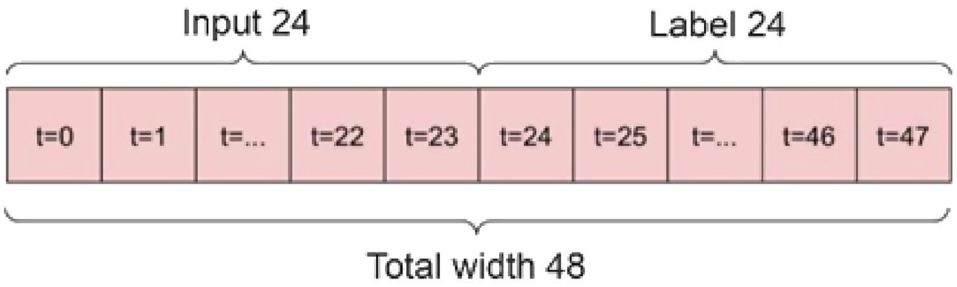

Fig. 1 Data window size representation

or non-essential columns streamlines the dataset, focusing on the variables crucial for the forecasting model. Data normalization and Data splitting part was done keeping the target variable, *MeanPower data* (Average normalized PV generation data).

2.4 Model inputs and outputs summary

Seperate models were used to forecast PV energy generation forecasting and wind speed, each using tailored input–output configurations after careful data preprocessing and feature engineering steps. Table 4 shows the inputs and outputs used in the models.

For PV Energy Forecasting, the input features include temperature, dew point, relative humidity, sea-level air pressure, wind vector components *(Wx, Wy)*, and temporal features (day and year sine and cosine signals). Wind speed is included as an input to understand its influence on solar power output. The output variable is the PV energy generation.

For Wind Speed Forecasting, the input features are temperature, dew point, relative humidity, sea-level air pressure, wind vector components *(Wx, Wy)*, and temporal features (day and year sine and cosine signals). In this model, wind speed is the output variable, reflecting the forecasted wind energy potential.

2.5 Data windowing

The objective of data windowing is to predict 24 h into the future based on the information from the preceding 24 h. By aligning the model's input and output windows, the training process enables the models to understand the temporal patterns and dependencies within the data, ultimately enhancing its ability to make accurate predictions for the specified time horizon. Therefore the total window consists of *input window* of size 24 and a *output/label window* of size 24 for both forecasting models as shown in Fig. 1, here *t* indicates time step. In this study, time series forecasting is done using TensorFlow.The models implemented in this study adopt a single-output, multi-time-step forecasting approach using single-shot models. In single output model, the model will predict only one feature (target feature), whereas multiple-output models will predict multiple features. In multi-step prediction, the model learns to predict a range of future values, differing from a single-step model where only a single future point is predicted. This distinction allows for the prediction of a sequence of future values.

3 Development of forecasting models

One high-level approach to this problem is to use a single-shot model, where the model makes the entire sequence prediction in a single step. This can be implemented efficiently using a dense layer. We used three models which are the baseline model, CNN model, and LSTM model.

3.1 Baseline model

The baseline model serves as a fundamental reference point for comparison. Typically, it involves simple statistical methods or straightforward algorithms. A repeat baseline model is used in this study where the task is to repeat the previous day, assuming tomorrow will be similar.

3.2 1-D CNN model

In the realm of time series forecasting, the CNN model stands out as a powerful architecture capable of extracting temporal patterns from sequential data. Unlike traditional neural networks, CNNs are adept at capturing local dependencies through convolutional operations.

3.2.1 1-D CNN model architecture

The CNN architecture for time series forecasting is designed to capture intricate temporal patterns in energy generation data as illustrated in the model flowchart Fig. 2. The architecture begins with a lambda layer that selects specific time steps from the input data, focusing on the most recent and relevant information for accurate forecasting.

Following this, the convolutional layer employs a kernel size, matching the input time steps, and uses Rectified Linear Unit (ReLU) activation to perform local operations on the sequential data, effectively extracting complex temporal features. Batch normalization is then applied to stabilize the training process by normalizing the inputs, which contributes to faster convergence and improved model performance.

To prevent overfitting, a dropout layer with a dropout rate of 0.01 is incorporated, selectively dropping connections during training to enhance the model's generalization capabilities. The dense layer, utilizing ReLU activation and He initialization, refines the features extracted by the previous layers, enhancing the model's understanding of temporal dependencies. Finally, the reshape layer adjusts the output to match the desired prediction sequence length, ensuring that the predictions align with the forecasting task.

3.2.2 Mathematical model

The 1D Convolutional Neural Network (CNN) model for both mean power generation and wind speed forecasting processes input data as a sequence of time steps $X = \{x_1, x_2, \ldots, x_T\}$, where each x_t represents a set of features at time step t.

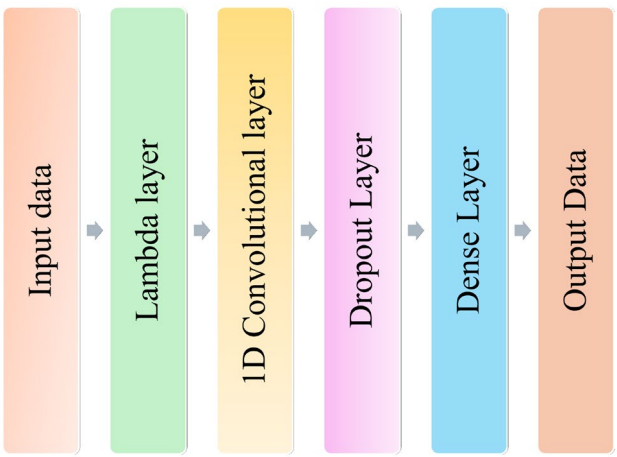

Fig. 2 CNN model architecture used for PV energy generation and Wind speed forecasting

The model begins with a Lambda layer that selects a fixed number of the most recent time steps from the input sequence, denoted as X_{selected}. Specifically, the Lambda layer operates as follows:

$$X_{\text{selected}} = X[:, -K\ :, :],$$

where K is the convolution width, the number of time steps considered for forecasting. This selected subset of the input sequence is then passed through the convolutional layer. The convolutional layer applies a filter w to the input sequence, producing an output y_t as follows:

$$y_t = \sum_{k=0}^{K-1} x_{t+k} \cdot w_k + b,$$

where K is the kernel size and b is the bias term. This output is passed through a ReLU activation function:

$$y'_t = \max(0, y_t).$$

Afterward, batch normalization is applied:

$$y''_t = \gamma \left(\frac{y'_t - \mu}{\sigma} \right) + \beta,$$

where μ and σ represent the batch mean and standard deviation, and γ and β are learnable parameters. Dropout is applied to prevent overfitting:

$$y'''_t = \text{Dropout}(y''_t).$$

The output is then passed through a dense layer:

$$y_{\text{pred}} = W \cdot y'''_t + b_d.$$

Finally, the output is reshaped to match the required prediction format:

$$\hat{Y} = \text{Reshape}(y_{\text{pred}}).$$

The model is trained by minimizing the MSE which is the loss function. This architecture is used for both forecasting tasks to predict future values based on historical data. This carefully structured design of each layer contributes to the 1-D CNN model's ability to accurately forecast energy generation by effectively capturing and analyzing relevant temporal patterns in the data.

3.3 LSTM model

The LSTM model is a specialized type of recurrent neural network (RNN) designed to address challenges related to learning long-term dependencies within sequential data. In the context of energy generation forecasting, the LSTM model proves valuable due to its ability to discern intricate patterns and trends in time-series data. The Fig. 3 shows the model architecture of the used LSTM models in this study in forecasting PV generation energy and wind speed.

3.3.1 LSTM model architecture

The architectural choices for the LSTM model are designed to optimize its ability to understand and forecast energy generation patterns. The LSTM layer is configured with a specific number of units to effectively learn and remember patterns across temporal sequences. This layer processes the input data and provides the final output at the last time step, capturing long-term dependencies crucial for accurate forecasting.

A dense layer is introduced with an initialization strategy, such as He initialization, to enhance the learning process. This layer outputs values that align with the desired prediction sequence length, refining the features learned by the LSTM layer and facilitating effective forecasting.

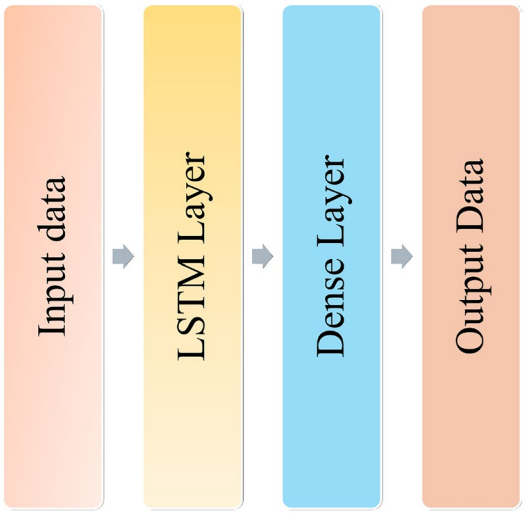

Fig. 3 LSTM model architecture used

The reshape layer tailors the output to meet the specific requirements of the forecasting task. This layer ensures that the predictions conform to the designated format by adjusting the shape of the output to match the expected sequence length.

These architectural choices ensure that the LSTM model is well-equipped to capture and forecast energy generation patterns accurately, leveraging its ability to learn from temporal dependencies and produce reliable predictions.

4 Training procedure followed

The training of neural network models involves several critical steps to ensure effective learning and performance evaluation. The MSE is used as the loss function, as it is suitable for regression tasks by quantifying the average squared difference between predicted and actual values. For efficient weight updates during training, the Adam optimizer is employed. The Adam optimizer has the ability to adjust learning rates and manage noisy data, making it especially useful for time-series forecasting, where changing data patterns require flexible and stable learning [45].

To monitor the model's performance, metrics such as MAE, RMSE, and R-squared (Coefficient of Determination) are used. These metrics help assess how well the model is performing, with R representing the actual value and P the predicted value. An epsilon value ($\epsilon = 10^{-7}$) is added in R^2 calculations to ensure numerical stability and prevent division by zero errors (Table 5).

The model was trained using the fit method with the training data. To manage training duration, the number of epochs was limited to a predefined maximum. Validation data was used to assess the model's performance on unseen data. Early stopping was applied to halt training if the validation loss did not improve within a specified patience period. This training process was encapsulated in a function to ensure consistent application across different neural network architectures. The training history, which provides insights into the model's learning progress, was recorded for further analysis and interpretation.

Table 5 Summary of evaluation metric equations

Evaluation metrics	Formulas
Root mean square error (RMSE)	$RMSE = \sqrt{\frac{1}{n}\sum_{i=1}^{n}(R_i - P_i)^2}$
Mean square error (MSE)	$MSE = \frac{1}{n}\sum_{i=1}^{n}(R_i - P_i)^2$
Mean absolute error (MAE)	$MAE = \frac{1}{n}\sum_{i=1}^{n}\lvert Y_i - \hat{Y}_i\rvert$
R^2 value (coefficient of determination)	$R^2 = 1 - \frac{\sum_{i=1}^{n}(R_i - P_i)^2}{\sum_{i=1}^{n}(R_i - \bar{R})^2 + \epsilon}$

Table 6 Data description of weather data

	temp	*dwpt*	*rhum*	*prcp*	*snow*	*wdir*	*wspd*	*wpgt*	*pres*	*tsun*	*coco*
Count	44,783	44,780	44,780	43,250	0	40,288	44,782	0	44,320	0	15,543
Mean	18.507	11.489	66.537	0.026	NaN	236.852	8.926	NaN	1015.731	NaN	3.139
Std	4.108	5.696	17.210	0.344	NaN	94.976	6.567	NaN	3.568	NaN	1.755
Min	3.9	– 20.7	4.0	0.0	NaN	0.0	0.0	NaN	999.3	NaN	0.0
Max	37.8	22.9	100.0	30.0	NaN	360.0	59.4	NaN	1032.5	NaN	25.0

Table 7 Weather data variables and missing value counts

Feature	Missing value count
temp	1
dwpt	4
rhum	4
prcp	1534
wdir	4496
wspd	2
pres	464

5 Results and discussion

This section presents the results obtained in this study, including relevant plots and their corresponding analyses. It provides conclusions drawn from the findings, along with discussions on the implications of these results. The focus is on interpreting the data, comparing model performances, and exploring how the outcomes contribute to the overall research objectives.

5.1 Weather data analysis results

Table 6 shows the data description table obtained in the initial EDA of weaher data. Looking at the *count* values, '*snow*,' '*wpgt*,' '*tsun*,' and '*coco*' features were excluded from the features list due to their minimal contribution or the availability of data points, making them unsuitable for meaningful analysis.

Missing values counts are shown in front of each of the remaining features as shown in Table 7. It can be observed that still, the missing values count is considerably high for *wdir* and *prcp*.

The *wdir* feature, representing wind direction, consistently shows missing values (NaNs) throughout the dataset particularly when wind speed (*wspd*) is zero. Since wind direction is undefined when there is no wind, these missing values refer to zero wind speed data points according to the reference data. For clarity, the last 10 data points are presented in Table S1, illustrating the occurrence of NaN values for instances of zero wind speed.

The pandas profiling heat map correlation plot (Fig. 4) was obtained to see the correlation of the *prcp* feature with others particularly due to its high missing values and decide if the feature is necessary or not. It can be observed that there are lighter colours meaning low correlations with the *prcp* feature. With substantial number of missing values and demonstrated weak correlations with the rest of the features in the heatmap, the decision was made to exclude the *prcp* feature from the dataset. This step aimed to enhance the model's reliability in accurate forecasting by focusing on features that provide more meaningful insights and reducing noise from the dataset.

Moreover, the heat map indicates significant relationships between *dwpt* and *temp*, *dwpt* and *rhum*, as well as *dwpt* and *press*, suggesting that these features are likely to contribute valuable information to the forecasting model. Therefore selected features were used in this process.

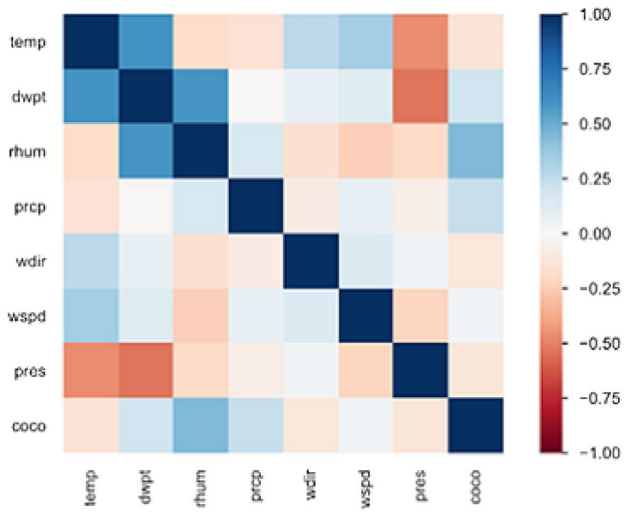

Fig. 4 Heat map correlation plot

5.2 PV generation data analysis results

A data description obtained in the EDA is shown in the Table 8. A closer look at the min values from the table revealed some negative values. Therefore to handle that, the negative values were replaced by their positive magnitude to ensure data consistency and align with the inherent nature of power generation. The variation in mean and standard deviation across the 10 PV generators is due to their different power ratings, which represent the maximum power each system can generate. Since the power ratings vary, this naturally leads to differences in the mean and standard deviation values. This diversity in power capacity shows the importance of considering the individual characteristics of each PV system when analyzing and interpreting the data. Taking these differences into account is essential for accurate assessments and insightful conclusions regarding the performance of each PV system within the microgrid.

The box plot was obtained for the EDA process of the PV data (Fig. 5). The tails of the plot indicate maximum peak values of PV generations over the years. Although these points appear as outliers, they represent valid extreme values rather than anomalies. Therefore, using suitable otlier detection techniques is essential to accurately identify true outliers and avoid misinterpreting extreme values as erroneous data.

5.3 Data preprocessing results

5.3.1 Wind data preprocessing

Since it was observed that the *wdir* feature contained a significant portion of missing values. These missing values corresponded primarily to instances where *wspd* was recorded as zero, making wind direction irrelevant. To handle these missing values, a potential solution was to integrate both wind direction and wind speed into a wind vector as a feature in future analyses. Additionally, for cases where wind speed equals zero, assigning a value of zero to the corresponding missing wind direction was done.

The remaining missing weather data values were handled using linear interpolation. Although the weather data may exhibit fluctuations over time, linear interpolation is still suitable for filling short-term gapse hourly data due

Table 8 Data description of PV combined data

	PV1	PV2	PV3	PV4	PV5	PV6	PV7	PV8	PV9	PV10
Count	169,796	169,792	152,537	138,499	157,844	136,167	178,033	178,042	178,036	178,050
Mean	7.693	6.268	15.346	5.495	57.871	8.183	24.883	12.867	27.246	11.104
Std	11.226	9.151	23.408	7.865	86.308	11.905	36.346	19.020	40.393	16.466
Min	0	0	− 0.119	0.003	− 0.759	0	− 0.259	− 0.068	− 0.606	− 0.001
Max	34.977	29.837	86.224	24.533	328.436	45.762	143.878	72.969	164.853	65.313

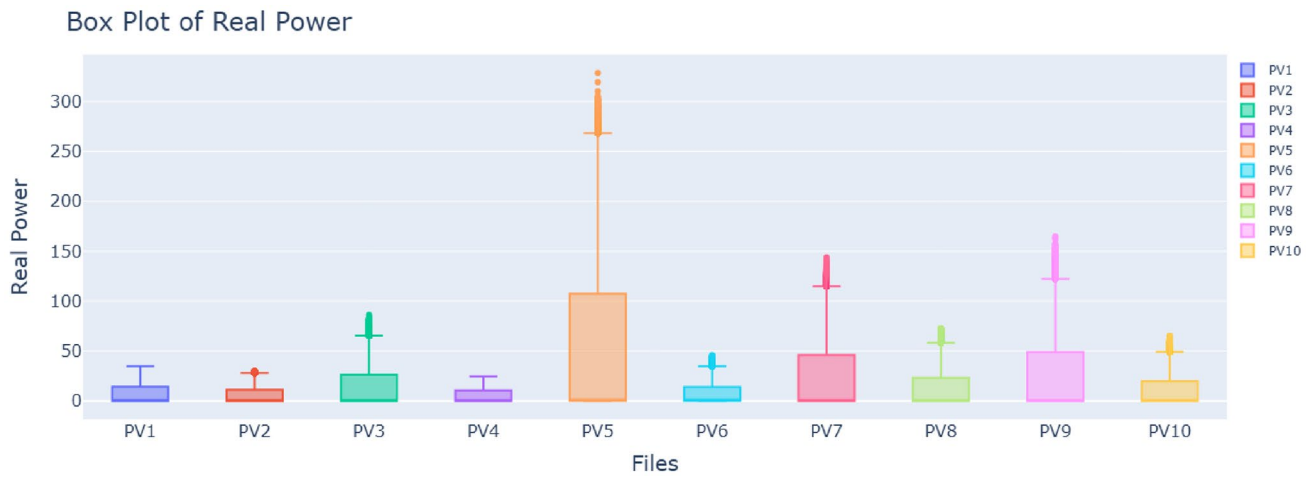

Fig. 5 Box plot for PV data

to the assumption that weather conditions generally change gradually within small time intervals [46]. Given the hourly nature of the data, this method aligns with the temporal continuity expected in meteorological data [47]. It provides a practical approach to filling missing values while preserving the integrity of the dataset for further analysis.

The two plots, Figs. 6 and 7, which display the complete dataset and a sample dataset, highlight the random and fluctuating patterns within the weather data.

In this study, the STL decomposition method (Seasonal-Trend decomposition using LOESS) which is a seasonal decomposition method, was employed for outlier detection. It breaks the time series into its seasonal, trend, and residual components, making it particularly useful for detecting outliers in the residuals after accounting for seasonality and trends. Upon reviewing the residuals from the STL decomposition, data points identified as potential outliers, at threshold value 5, which is five times the standard deviation, were visually inspected and confirmed that they are not obvious outliers because of alignment with the data pattern. The threshold value was considered by visualizing the amount of anomaly detected. Therefore, no replacements were made for any data.

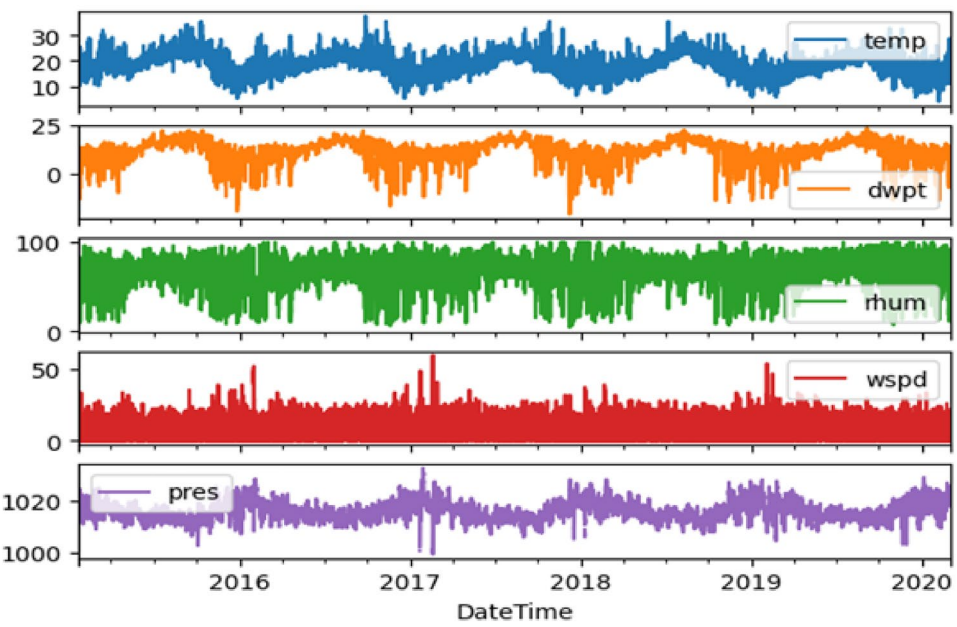

Fig. 6 Line plot of weather data over time

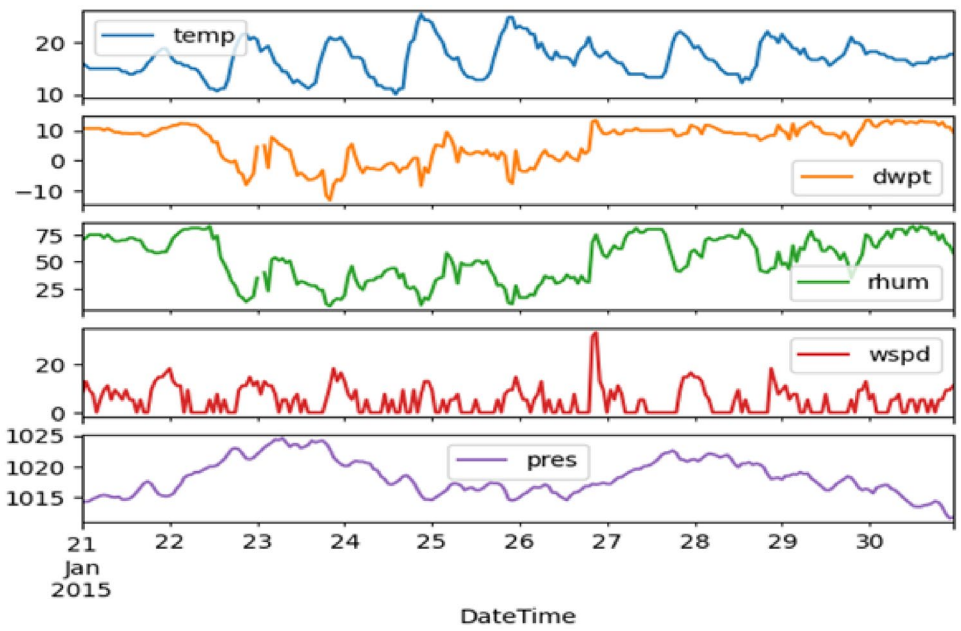

Fig. 7 Sample of last 10 days of weather data over time

5.3.2 PV generation data preprocessing

From the initial EDA, negative values and missing values were observed in the 10 PV Generators data. Also, it was noted that starting dates were different in the 10 datasets. Upon reviewing negative data values along with their corresponding datetime entries, it became evident that a potential criterion for replacement could involve substituting negative values with their respective magnitudes. An examination of the data plots was conducted to determine an appropriate method for filling in missing values and detect obvious outliers.

The analysis of the last 20 days of data (Feb 10, 2020–Feb 29, 2020) from the PV generators showed similar patterns across datasets, despite differences in maximum power generation (Figures S1, S2). This similarity suggests that normalizing the data by mapping it to the same range is essential to highlight inherent patterns and make the data comparable across different generators.

Outlier detection in the PV generation data was conducted using time series decomposition, similar to the approach for weather data. A threshold of 5.0, corresponding to five times the standard deviation of residuals, was applied to identify anomalies. Assuming a daily pattern of PV generation, seasonality was set to 24 data points. Example plots for the *PV8* generator (Figure S3) and zoomed-out perspectives (Figure S4) effectively illustrate the detected anomalies across the datasets.

A review of residuals plot in STL decomposition revealed that points identified as outliers at five times the standard deviation often exhibit similarities with neigbouring values upon visual inspection, challenging their classification as significant anomalies. This suggests these points are not true anomalies but rather normal fluctuations in PV energy generation, highlighting the risk of misclassifying valid data as outliers.

The variance in mean and standard deviation among the 10 PV generators reflects differences in their power ratings, which define each generator's maximum output. These variations underscore the need to account for individual generator characteristics in data analysis. To ensure consistency and comparability, the data was normalized to a 0–1 range using the Min-Max scaler, allowing accurate assessments while respecting the inherent differences in power capacity across generators.

Following the data normalization, notable differences in box plot distributions were observed, even among PV generators in the same geographical area. These variations were attributed to differences in data collection start times and environmental conditions, such as shadowing effects, across stations. These factors significantly influenced the distribution patterns, underscoring the importance of carefully selecting input data for forecasting models.

The alignment of PV generation data with generalized weather data from San Diego Airport highlighted the need to account for regional variations to improve interpretation accuracy. To enhance model adaptability and reliability,

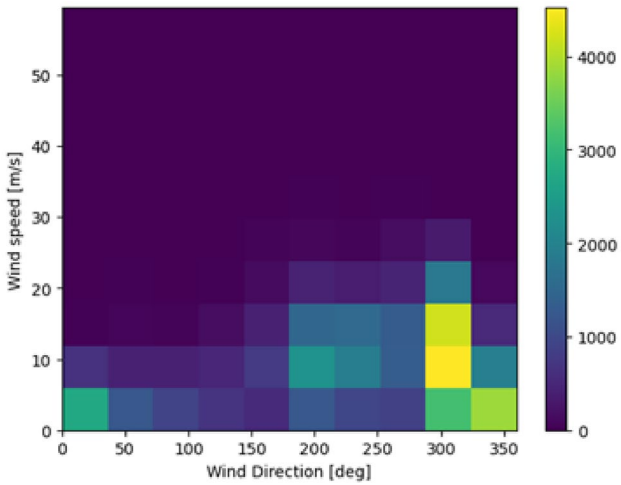

Fig. 8 Heat map of wind speed with wind direction

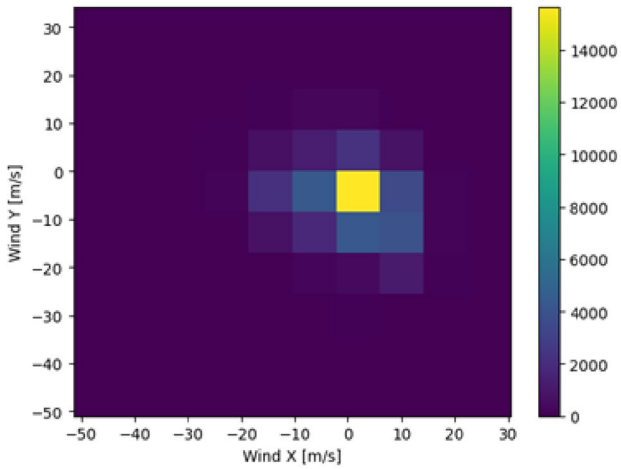

Fig. 9 Distribution of wind vectors heat map

the normalized PV generation values from all generators were averaged by datetime, creating a more comprehensive dataset. This averaging process also helped address outliers, thereby improving the overall data quality.

5.4 Feature engineering results

5.4.1 Weather data feature engineering

wdir (deg)-gives the wind direction in units of degrees. Angles do not make good model inputs: 360° and 0° should be close to each other and wrap around smoothly. And also the direction shouldn't matter if the wind is not blowing. Figure 8 shows the initial data distribution along with wind speed and wind direction. The color represents the number of data points corresponding to the region. Recognizing the challenges posed by traditional angular measurements, a more interpretable approach involves converting wind direction and wind speed columns into a wind vector.

This transformation aligns with the concept that 360° is equivalent to 0° in circular measurements. By representing the data in terms of wind vectors, the model gains a simpler and more accurate interpretation of the distribution. This not only enhances the model's understanding but also contributes to improved performance in capturing the nuances of wind-related features. The distribution of wind vectors are shown in Fig. 9.

The *Date Time* column is valuable but is not optimally represented in its string form. To enhance its utility, the first step involves converting it into seconds. However, treating time in seconds directly may not offer meaningful insights for the model. Given the inherent daily and yearly periodicity in weather data and simultaneously weather parameters leading to periodicity in generation data, addressing this periodic nature is crucial. To extract usable signals, a strategic approach involves employing sine and cosine transforms. This technique effectively clears the "Time

of day" and "Time of year" signals, providing the model with more interpretable and relevant temporal features for improved accuracy in capturing time related patterns. Figures 10 and 11 shows the day and year signals obtained with sine and cosine curves. The following two equations show the relationship of day and year with seconds.

$$day = 24 * 60 * 60$$
$$year = (365.2425) * day.$$

When the frequencies are unknown, a robust method involves utilizing the Fast Fourier Transform (FFT) to extract important frequency features. This technique allows the model to identify and leverage key frequencies of the features that contribute significantly to the underlying patterns in the data revealing prominent peaks near frequencies corresponding to 1/year and 1/day. Figure 12 shows the FFT for the *dew point*. Similarly, the plots can be obtained for other features and check for important frequencies for all the features. It can be observed that yearly and daily frequency is significant.

The features which are considered for forecasting after the feature engineering are *temp, dwpt, rhum, wspd, pres, Wx, Wy, Day sin, Day cos, Year sin* and *Year cos*.

5.5 Model hyperparameters and parameters

The values for key hyperparameters were carefully selected through iterative experimentation to ensure the optimal configuration of the models for accurate and reliable predictions.

The Table 9 below summarizes the hyperparameters and parameters used for the 1D CNN models applied to Wind Speed and PV Power forecasting.

For the 1-D CNN models, hyperparameter tuning was performed to improve their performance in energy generation forecasting. The convolution width was set at 12 for wind speed forecasting and 15 for PV energy forecasting to capture relevant temporal patterns, while the number of convolutional filters was adjusted to 256 for wind and 128 for PV. The kernel size was set similarly to the convolution width for both cases. The dropout rate was tuned to 0.01 for regularization. These values were chosen to strike a balance between model complexity and generalization, ensuring optimal performance in forecasting energy generation.

Similarly, LSTM models underwent hyperparameter tuning to improve their ability to capture temporal dependencies. The number of LSTM units was set to 128 for both wind speed and PV energy forecasting, allowing the models to retain sufficient memory and capture intricate patterns for both types of forecasting tasks.

Fig. 10 Day signal

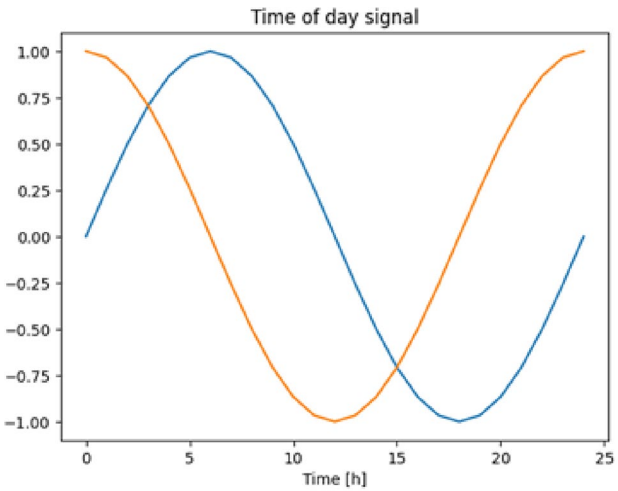

Table 9 Hyperparameters and parameters for 1-D CNN models in wind speed and PV power Forecasting

Parameter	PV energy forecasting	Wind speed forecasting
Batch size	32	32
Convolution width	12	15
Conv1D filters	256	128
Kernel size	12	15
Activation function	ReLU	ReLU
Dropout rate	0.01	0.01
Optimizer	Adam	Adam
Loss function	MSE	MSE
Metrics	MAE, RMSE, R^2	MAE, RMSE, R^2
Max epochs	200	200
Early stopping patience	10	4
Kernel initialization	He Normal	He Normal
Batch normalization	Yes	Yes
Dense layer units	24 (output steps)	24 * 1 (output steps)
Reshape output	24, 1	24, 1

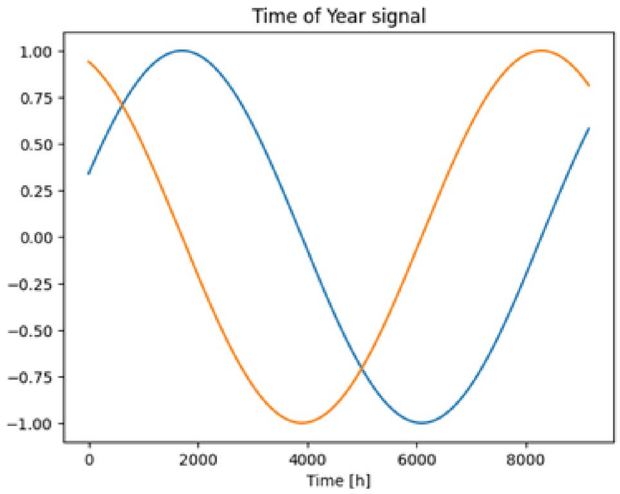

Fig. 11 Year signal

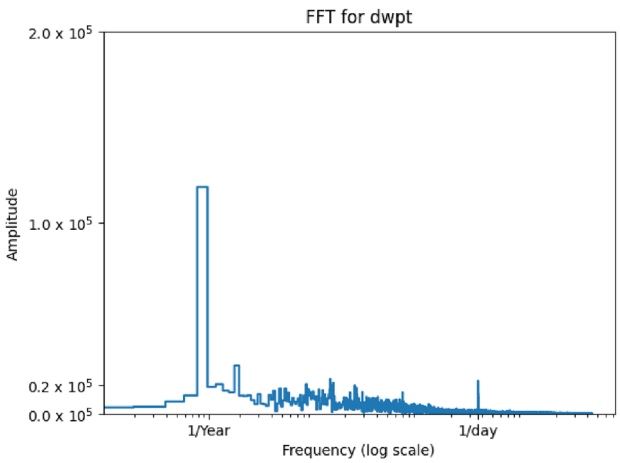

Fig. 12 example of FFT: for *dwpt* feature

Table 10 Test data performance evaluation of wind speed forecasting models

model	MSE	MAE	RMSE	R2value
RepeatBaseline	38.637	4.505	6.215	0.112
CNN	21.354	3.621	4.621	0.448
LSTM	22.972	3.723	4.792.161	0.409

Table 11 Test data performance evaluation of PV generation forecasting models

model	MSE	MAE	RMSE	R2value
RepeatBaseline	1.149	0.832	1.071	0.087
CNN_model	0.005	0.034	0.072	0.899
LSTM_model	0.005	0.043	0.077	0.887

5.6 Performance evaluation of the models

Following hyperparameter tuning, the performance of all three models (CNN, LSTM, and Repeat Baseline) was evaluated across three datasets (training, validation, and test) for both wind speed and PV generation forecasting. The results of these evaluations are presented in the following sections.

The Table 10 shows the relevant metric values of the corresponding forecasting model on test data (unseen data) of wind data. From the table we can see that CNN model has outperformed the other two models.

The Table 11 shows the relevant metric values of the corresponding forecasting model on test data(unseen data) of PV generation data. From the table we can see that CNN model has outperformed other two models.

Furthermore looking at figures: Figs. 13 and 14, we can conclude the following,

- *Loss performance:* The Neural Network models demonstrate a very good loss performance on PV generation data compared to the baseline model. After hyperparameter tuning, the CNN model, in particular, shows the best performance in terms of the loss function.
- *MAE performance:* When assessing MAE on wind data, the Neural Network models again show better performance than the baseline model after hyperparameter tuning. Interestingly, the Neural Network models perform better on unseen data compared to the train and validation data, a trend not observed in the baseline model. The CNN model leads in MAE performance among all models.
- *RMSE performance:* For RMSE on wind data, the Neural Network models outperform the baseline model post-tuning. Similar to MAE, the unseen data yield better performance than the train and validation sets in Neural Network models. The CNN model is the best performer in terms of RMSE.
- *R2 performance:* The R2 performance of Neural Network models on wind data is significantly better than the baseline model after tuning, though the values hover around 0.4. Among the Neural Network models, the CNN model achieves the highest R2 values.

These results highlight the effectiveness of neural network models, particularly the CNN model, in forecasting renewable energy generation. The improved performance on unseen data underscores the robustness and potential of these models for real-world applications.

The evaluation of neural network (NN) models on PV and wind generation data shows significant improvement over the baseline model after hyperparameter tuning. The CNN model consistently outperforms other models when considering different performance metrics.

5.6.1 Computational performance evaluation

The computational efficiency of the models were assessed based on key performance metrics, including training time, inference time per sample, memory usage and scalability as shown in Table 12. Training time represents the total duration required for model convergence, while inference time measures the prediction speed per sample.

Table 12 Computational performance of forecasting models

Metric	1-D CNN (PV)	LSTM (PV)	1-D CNN (Wind)	LSTM (Wind)
Train time (h)	0.02	0.07	0.02	0.08
Inference time (ms)	220.32	262.00	190.55	353.43
Memory usage (GB)	0.93	1.03	1.12	1.15
Scalability	Low	Low	Low	Low

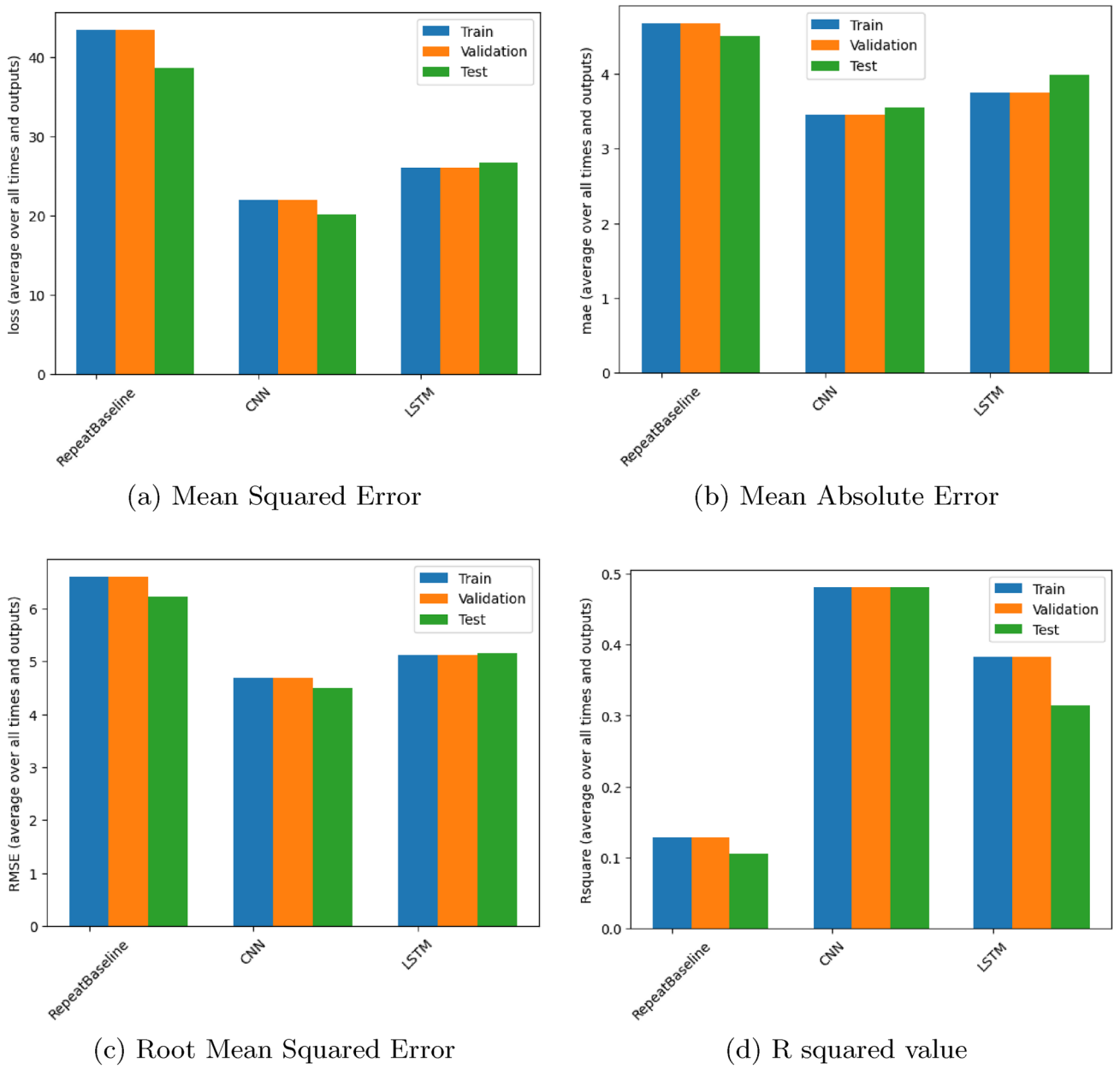

Fig. 13 Performances of wind forecasting models

Memory usage indicates the resource consumption during model execution, and scalability is determined based on the batch size. A lower batch size of 32 was selected to ensure stable training, avoid memory overflow, and improve generalization, especially given the temporal complexity of energy forecasting.

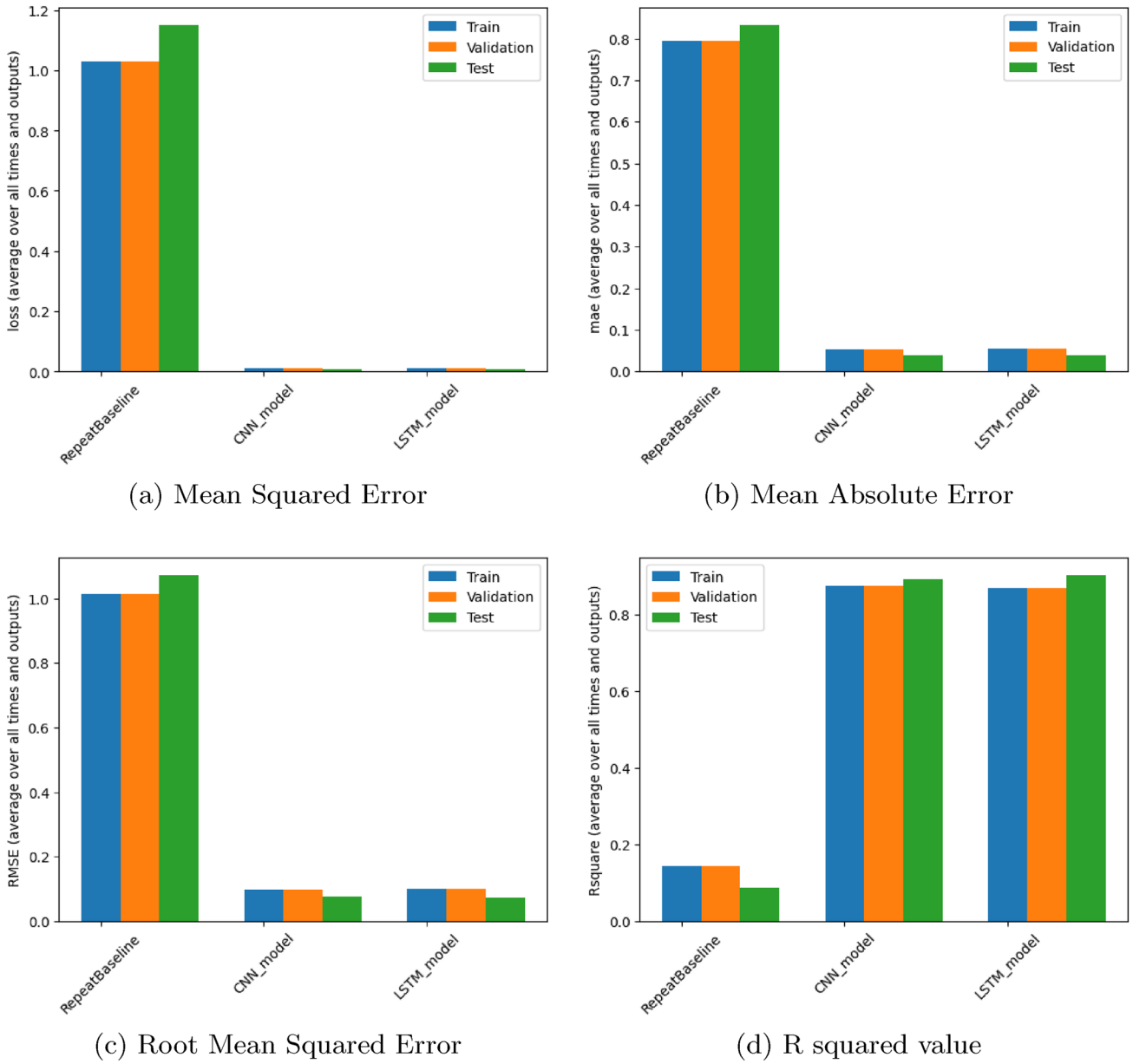

Fig. 14 Performances of PV energy generation forecasting models

The results demonstrate that the proposed 1-D CNN model significantly outperforms the LSTM model in terms of computational efficiency. The 1-D CNN model achieves faster training times, lower inference times, and reduced memory consumption. This better performance can be attributed to the 1-D CNN's ability to efficiently extract spatial-temporal patterns with convolutional filters while maintaining a lower computational burden compared to the recurrent nature of LSTMs, which require sequential processing. Furthermore, the 1-D CNN model provides a better trade-off between accuracy and efficiency, making it a more suitable choice for real-time energy forecasting applications where rapid predictions and resource efficiency are important.

5.7 Over-fitting and under-fitting

Over-fitting is a common challenge in machine learning where a model becomes overly attuned to the nuances and details of the training data, including noise and outliers, at the expense of its ability to generalize to new, unseen data.

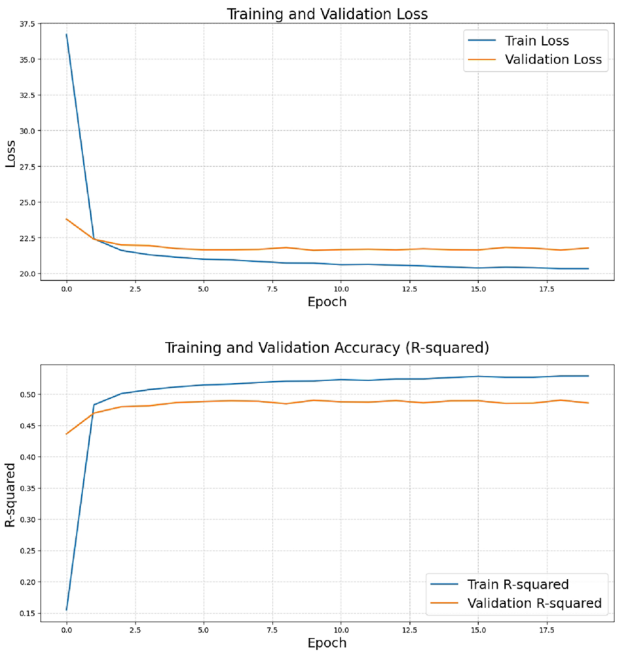

Fig. 15 Accuracy vs loss performances on train and validation data sets over epochs on wind speed forecasting CNN model

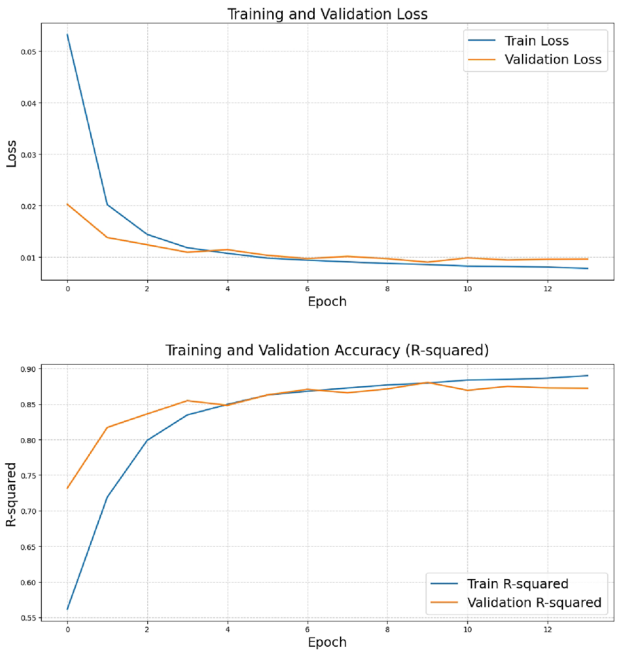

Fig. 16 Accuracy vs loss performances on train and validation data sets over on PV generation data forecasting CNN model

Under-fitting occurs when a model is too simplistic, failing to capture the intricate patterns within the data. This results in poor performance on both the training and testing datasets.

To check for over-fitting or under-fitting cases, the accuracy(R2 value) of the model and the loss performance(MSE) are plotted for training and test data(unseen data) over the epochs. Figures 15 and 16 shows the two plots which were plotted for the CNN models for PV generation and wind data respectively. In both figures, it can be seen that the both test and train accuracy increases over epochs while both losses getting decreased. Forecasting plots suggest a well-balanced learning process, showcasing the model's ability to learn from the training data while maintaining strong generalization to validation or testing datasets.

Our results demonstrate the effectiveness of our 1-D CNN models in differentiating between developing a learning machine and memorizing data. In machine learning, the distinction between developing a robust learning model and merely memorizing data is critical to addressing overfitting and underfitting. To mitigate these overfitting or underfitting

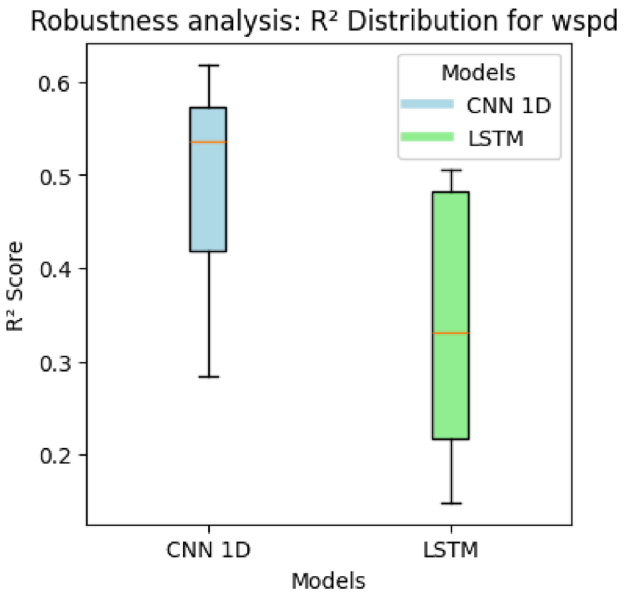

Fig. 17 R^2 distribution for wind speed forecasting (1D CNN vs. LSTM)

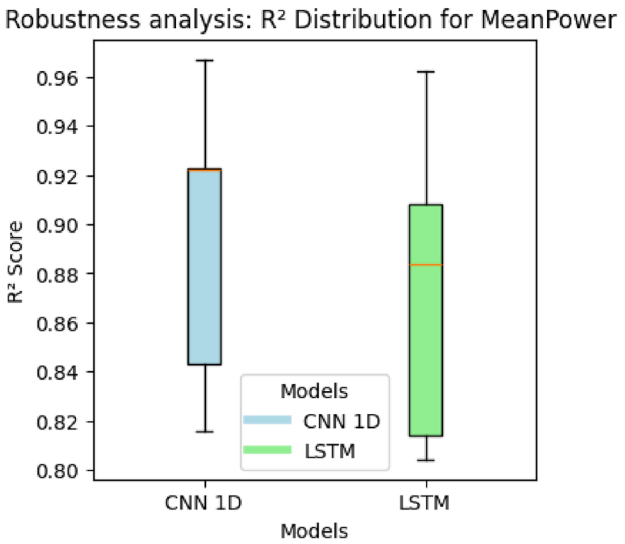

Fig. 18 R^2 distribution for PV energy forecasting (1D CNN vs. LSTM)

issues, we employed techniques such as dropout regularization (rate = 0.01), batch normalization, and early stopping, ensuring the model learned meaningful patterns rather than memorizing data. Our 1-D CNN model demonstrated better generalization capabilities compared to lSTM and baseline models, as evidenced by consistent improvements in loss and accuracy (R^2) on both training and validation sets, as shown in Table 10 and Fig. 14. By carefully tuning hyperparameters, including a convolution width of 15 for PV and 12 for wind, and using appropriate data splitting (70% training, 20% validation, 10% testing), we ensured the model captured temporal dependencies in renewable energy data without overfitting. The model's performance on unseen test data, visualized in ?? further validated its ability to track fluctuations and predict PV generation and wind speed accurately. This approach highlights the importance of balancing model complexity and generalization, enabling reliable and accurate forecasting for microgrid applications.

5.8 Robustness analysis of models

To evaluate the robustness of 1D CNN and LSTM models for wind speed and PV energy forecasting, we analyzed their performance using the R^2 score, as shown in the box plots (Figs. 17 and 18). For wind speed forecasting, the 1D CNN model achieved a median R^2 score of ~0.45 with a narrow interquartile range (IQR), indicating consistent performance,

while the LSTM model had a higher median R^2 score of ~0.5 but a wider IQR, showing greater variability. This suggests that the 1D CNN model is more robust and reliable for wind speed forecasting. For PV energy forecasting, both models performed well, with median R^2 scores of ~0.92 (1D CNN) and ~0.94 (LSTM). However, the 1D CNN model exhibited slightly better consistency with a narrower IQR, making it a practical choice despite the LSTM's marginally higher accuracy. Overall, the 1D CNN model is more robust and efficient, particularly for real-time applications, while the LSTM model excels in capturing complex temporal dependencies. These insights help guide model selection based on the specific requirements of the forecasting task.

5.9 Overall overview

The following two Figs. 19 and 20 show the simple visualization of the 3 split window samples of the test datasets in PV generation forecasting and Wind speed forecasting. The plots include inputs, labels and predictions clearly.It can be observed that the CNN models have captured the complex patterns of the data in a good way from the plots.

Lets look at the actual and predicted plot for last 15 days of Wind speed forecasting and PV energy forecasting CNN model.

It can be observed from Fig. 19 that the fluctuation is very high for wind speed however the model has been able to capture the variation up to some extent.

From Fig. 20 it can be observed that the fluctuation has a very uncertain special pattern for PV generation. The model has been able to capture the variation very much closely.

A notable observation in wind data plot is the high level of fluctuation in wind speed. Despite the inherent unpredictability associated with wind speed variations, the CNN model gives a commendable performance by capturing the variability to a considerable extent.

Actual data and the predicted data is plotted in the same graph to visualize the predictions. In figure Figs. 21 and 22 shows the plots for last 15 days for PV energy generation and wins speed respectively. In PV generation data plot, a distinct pattern of uncertain fluctuations in PV generation can be seen. Remarkably, the CNN model demonstrates a close alignment with the observed variations, showcasing its ability to accurately capture the nuanced patterns in PV energy generation. Meanwhile wind speed forecasting plot shows that wind has a uncertain pattern but the model has been able to closely identify the pattern.

These visualizations underscore the robust performance of the CNN model in both wind speed and PV energy forecasting, effectively navigating the challenges posed by the intricate and dynamic nature of environmental data.

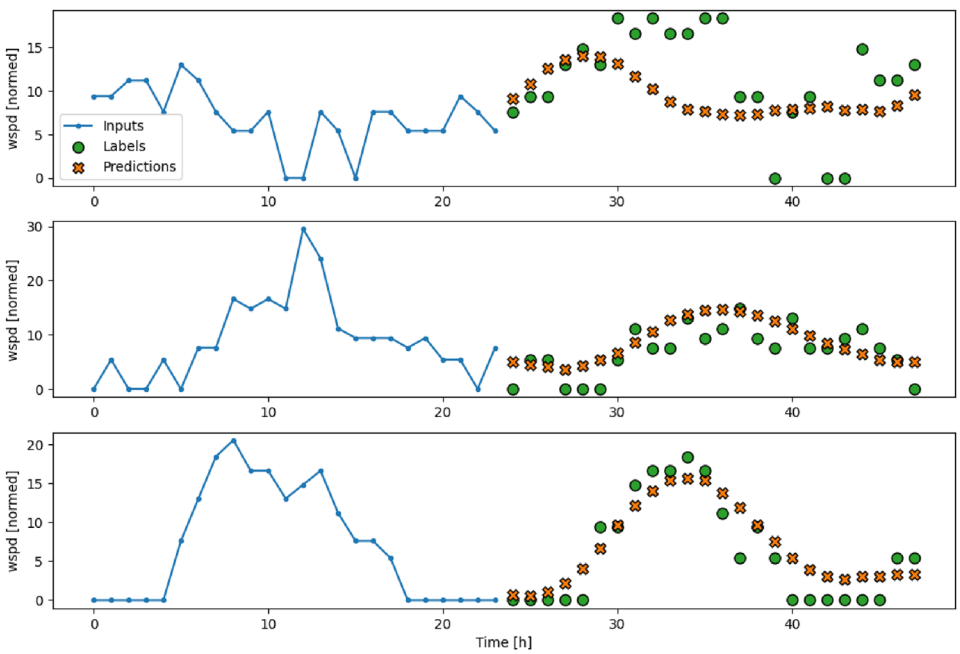

Fig. 19 split window samples of the test dataset on wind speed forecasting CNN model

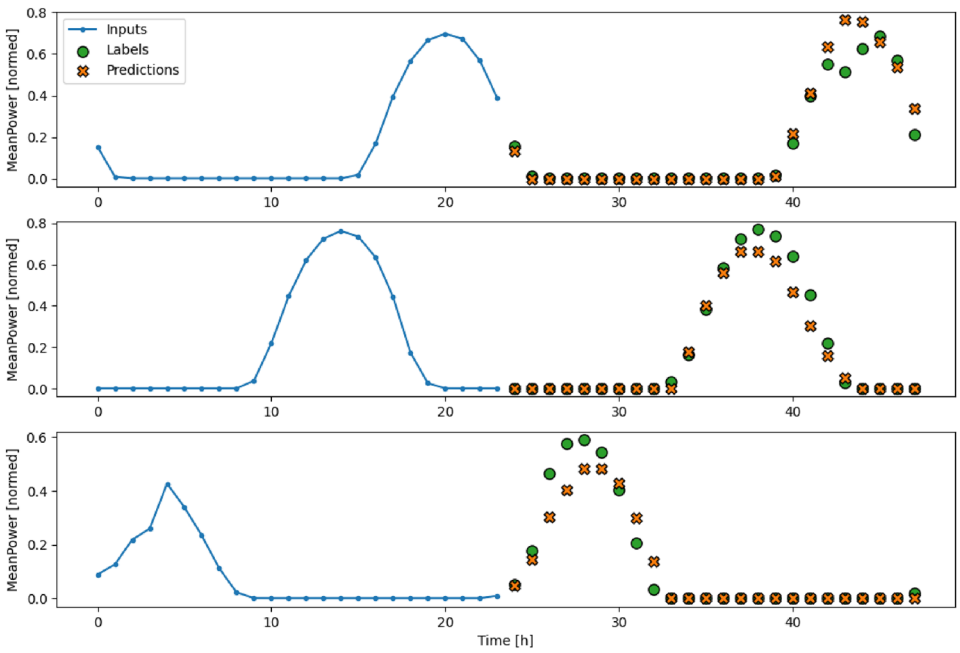

Fig. 20 split window samples of the test dataset on PV generation forecasting CNN model

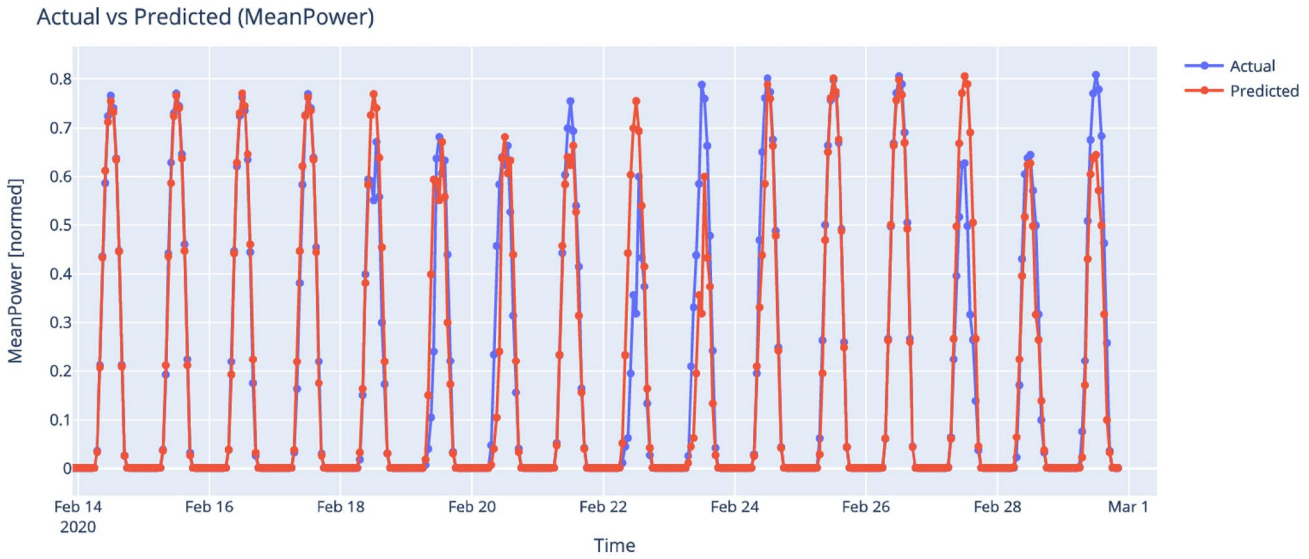

Fig. 21 Actual and predicted plot for last 15 days on test dataset of PV energy generation forecasting CNN model

The models' capability to closely track fluctuations enhances their reliability in predicting future values, contributing to the efficacy of renewable energy forecasting in practical applications.

The actual vs predicted values on the horizontal and vertical axes respectively are plotted further to see the predictions as in Fig. 23. The plot shows most data points are closer to the best fit line, which indicates there is less variation of predicted values with actual values and the best fit line angle is 40.98, which is closer to 45 degree (ideal).

6 Conclusions

This research explored the use of machine learning to forecast renewable energy generation and improve the operation of microgrids, which are small-scale power grids. The main challenge is that renewable energy sources, like solar and wind power, are variable and hard to predict. Our results highlight the advantages of 1-D CNNs over LSTMs for time

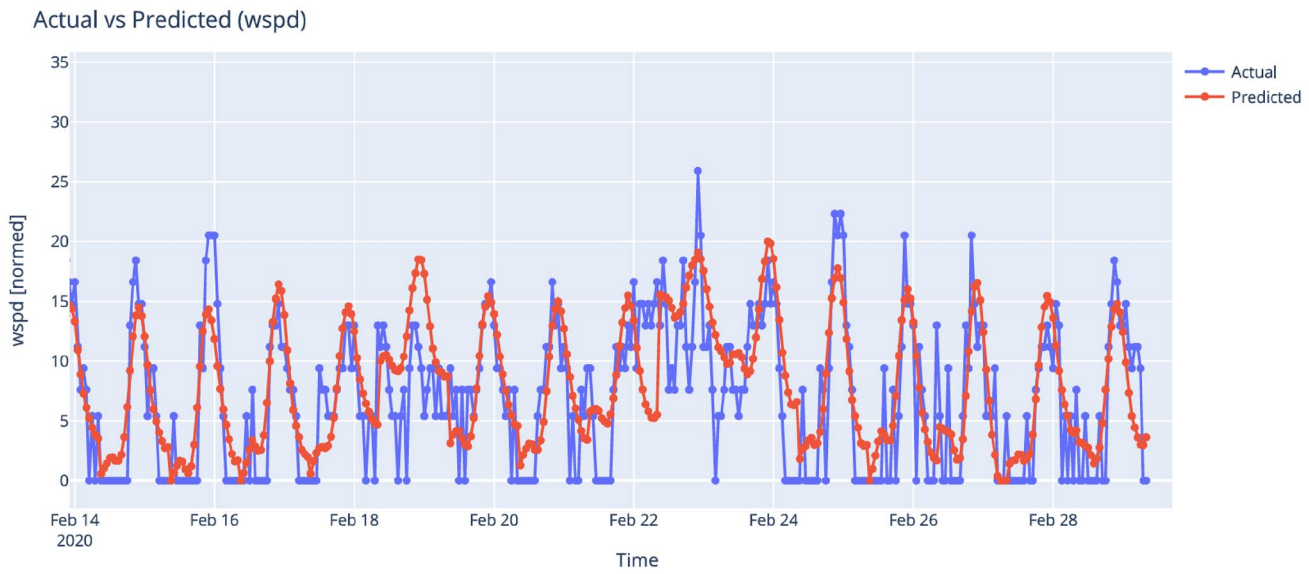

Fig. 22 Actual and predicted plot for last 15 days on test dataset of wind speed forecasting CNN model

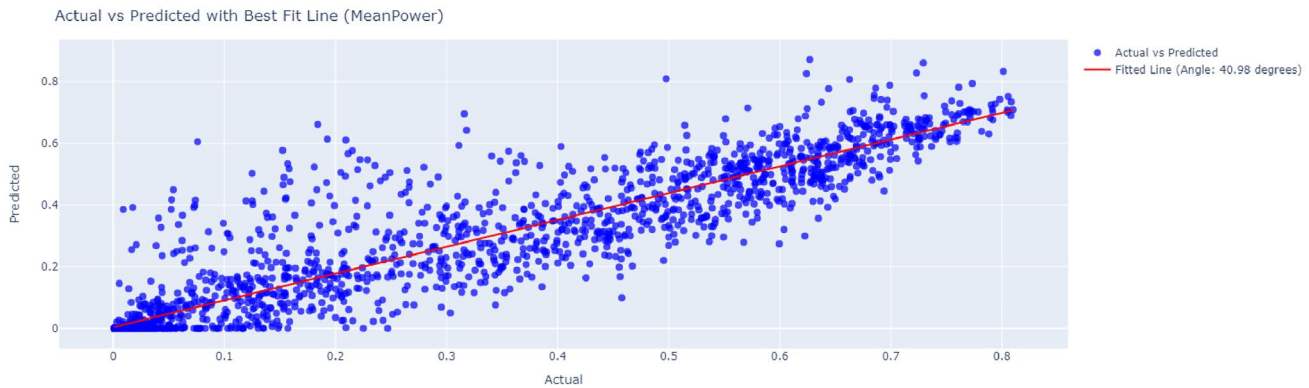

Fig. 23 Actual vs predicted plot with best fit line for PV generation test data on CNN model

series forecasting. Studies demonstrate the speed and effectiveness of 1-D CNNs in handling imbalanced datasets, showing that they can process data more quickly and efficiently than LSTMs [48]. Additionally, 1-D CNNs are found to capture localized features more efficiently and are less computationally intensive, making them ideal for applications where computational resources are limited [49]. Faster training times for 1-D CNNs make them suitable for real-time feature extraction in time series data, which is crucial for applications like renewable energy forecasting [50]. Moreover, the lower computational complexity of 1-D CNNs makes them advantageous for real-time applications, ensuring timely and accurate predictions [36].

By applying machine learning techniques, especially 1-D CNNs, to weather data from San Diego airport and renewable energy generation data from a microgrid in San Diego, the project was able to improve the accuracy of energy predictions. The CNN model performed better than both a baseline model and an LSTM model, demonstrating its potential in renewable energy forecasting. The results of this study contribute to the field of renewable energy forecasting. The success of the CNN models shows they can be useful tools for optimizing energy production and consumption in real-world applications. Accurate forecasting is crucial as we move towards sustainable and resilient energy systems.

6.1 Limitations

While this study demonstrates the effectiveness of 1-D CNNs for renewable energy forecasting, there are opportunities for further refinement. The dataset is geographically limited to San Diego, which may affect the generalizability of the

results to other regions. Additionally, while 1-D CNNs excel at capturing localized patterns, they may not fully model long-term dependencies in time series data. Finally, the models were tested on historical data, and their performance in real-time dynamic environments remains to be evaluated.

6.2 Future work

Future research could explore higher-resolution data intervals (e.g., 15-min increments) to improve forecasting accuracy while maintaining optimal computational efficiency. Given the demonstrated performance of 1D CNN models, researchers could develop more advanced hybrid models that incorporate 1D CNNs to balance computational cost and performance effectively. For instance, hybrid architectures combining 1D CNNs with LSTMs or integrating physics-based models could help address long-term dependency challenges. Additionally, researchers could evaluate the robustness of these models by testing them on datasets from both higher-capacity and lower-capacity microgrids. Incorporating additional data sources and validating the models on datasets from diverse geographic regions would further enhance their generalizability and robustness. Finally, real-time testing in operational microgrids would provide valuable insights into the practical applicability of these models.

In summary, this research shows the potential of 1-D CNN models in short term forecasting renewable energy generation for optimizing microgrid operation. It provides valuable insights and highlights future research opportunities. The findings of this study can guide future work in renewable energy management and help move towards a more sustainable future.

Acknowledgements This research was supported by the Science and Technology Human Resource Development Project, Ministry of Education, Sri Lanka, funded by the Asian Development Bank (Grant No. STHRDP/CRG/R2/RJ2)

Author contributions Piyumi Sudasinghe conducted data acquisition, data preprocessing, data analysis, and drafting the initial version of the manuscript; Dr. Damayanthi Herath contributed to conceptualization of the work, research supervision, data analysis and drafting the manuscript. Isiwara Karunarathne and Dr. Hansani Weerathunge contributed to data analysis. Dr. Lahiru Jayasooriya contributed to data analysis and funding acquisition. All authors read and approved the final manuscript.

Data availability This study is performed based on PV power generation data from the University of California, San Diego MicroGrid [3] and weather data from San Diego International Airport [15].

Code availability Codes written during the current study are available from thecorresponding author on request.

Materials availability Materials used during the study are available from thecorresponding author upon request.

Declarations

Ethics approval and consent to participate Not applicable.

Competing interests The authors declare that they have no competing interest.

References

1. Benti NE, Chaka MD, Semie AG. Forecasting renewable energy generation with machine learning and deep learning: current advances and future prospects. Sustainability. 2023;15(9):7087.
2. Karunarathne MGIU, Sudasinghe PB, Weeratunge HY, Herath D. Improving microgrid energy demand forecasting using convolutional neural networks. Engineer J Inst Engineers Sri Lanka. 2024;57(4):1–10.
3. Khayaty MS, Movludiazar A, Fotouhi R. Intelligent microgrid energy management system based on deep learning approach. In: 2021 11th Smart Grid Conference (SGC). ResearchGate. 2021.
4. Silwal S, Mullican C, Chen Y-A, Ghosh A, Dilliott J, Kleissl J. Open-source multi-year power generation, consumption, and storage data in a microgrid. J Renewable Sustain Energy. 2021;13(2): 025301.

5. Raja SSS, Ahmad A, Alqaraghuli MA, Gao W. A review on the application of machine learning techniques for renewable energy forecasting. Renew Sustain Energy Rev. 2021;149: 111367.
6. Maduabuchi C, Nsude C, Eneh C, Eke E, Okoli K, Okpara E, Idogho C, Waya B, Harsito C. Renewable energy potential estimation using climatic-weather-forecasting machine learning algorithms. Energies. 2023;16(4):1603.
7. Saini VK, Kumar R, Al-Sumaiti AS, Heydarian-Forushani E. Learning based short term wind speed forecasting models for smart grid applications: an extensive review and case study. Electric Power Syst Res. 2023;222: 109502.
8. Zhang Y, Zou Y, Li X, Wang J. Microgrid energy management strategy considering source-load forecast error. Int J Electr Power Energy Syst. 2025;164: 110372.
9. Widodo DA, Iksan N, Udayanti ED, Djuniadi. Renewable energy power generation forecasting using a deep learning method. IOP Conf Ser Earth Environ Sci. 2021;700: 012026.
10. Aupke P, Kassler A, Theocharis A, Nilsson M, Uelschen M. Quantifying uncertainty for predicting renewable energy time series data using machine learning. Eng Proc. 2021;5(1):50.
11. Heydari A, Astiaso Garcia D, Keynia F, Bisegna F, De Santoli L. Renewable energies generation and carbon dioxide emission forecasting in microgrids and national grids using grnn-gwo methodology. Energy Proc. 2019;159:154–9.
12. Ali M, Ahmad M, Koondhar MA, Akram MS, Verma A, Khan B. Maximum power point tracking for grid-connected photovoltaic system using adaptive fuzzy logic controller. Comput Electr Eng. 2023;110: 108879.
13. Ali M, Vasquez JC, Guerrero JM, Guan Y, Golestan S, Cruz JDL, Koondhar MA, Khan B. A comparison of grid-connected local hospital loads with typical backup systems and renewable energy system based ad hoc microgrids for enhancing the resilience of the system. Energies. 2023;16(4):1918.
14. Bird L, Milligan M, Lew D. Integrating variable renewable energy: challenges and solutions. Technical report, National Renewable Energy Laboratory (NREL). Technical Report 2013.
15. Gayen D, Chatterjee R, Roy S. A review on environmental impacts of renewable energy for sustainable development. Int J Environ Sci Technol. 2024;21(1–2):5285–310.
16. Miller LM, Keith DW. Climatic impacts of wind power Joule. 2018;2(12):2618–32.
17. Sweeney-Lejeune L, Browell J, McMillan D. The future of forecasting for renewable energy. Wiley Interdiscip Rev Energy Environ. 2020;9(6):375.
18. Kim J-H, Kim J-H, Kim J-H. A deep learning-based forecasting model for renewable energy scenarios to guide sustainable energy policy: a case study of korea. Renew Sustain Energy Rev. 2020;121: 109688.
19. Ahmed F, El-Shafie A, Jaafar O. A review of deep learning for renewable energy forecasting. Energy Convers Manage. 2019;198: 111814.
20. Rodríguez F, Fleetwood A, Galarza A, Fontan L. Predicting solar energy generation through artificial neural networks using weather forecasts for microgrid control. Renewable Energy. 2018;126:855–64.
21. Husein M, Chung I-Y. Day-ahead solar irradiance forecasting for microgrids using a long short-term memory recurrent neural network: a deep learning approach. Energies. 2019;12(10):1856.
22. Saini VK, Singh R, Mahto DK, Kumar R, Mathur A. Learning approach for energy consumption forecasting in residential microgrid. In: 2022 IEEE Kansas Power and Energy Conference (KPEC), 2022:1–6.
23. Abdelkawy NA, Shammre ASA. Machine learning models for solar power generation forecasting in microgrid application: implications for smart cities. Sustainability. 2024;16(14):6087.
24. Meenal R, Binu D, Ramya KC, Michael PA, Kumar KV, Rajasekaran E, Sangeetha B. Weather forecasting for renewable energy system: a review. Arch Comput Methods Eng. 2022;29:2875–91.
25. Saini VK, Mathur F, Gupta V, Kumar R, Mathur A. Predictive analysis of traditional, deep learning and ensemble learning approach for short-term wind speed forecasting. In: 2020 IEEE International Conference on Computing, Power and Communication Technologies (GUCON) 2020:783–788.
26. Kong X, Chen Z, Liu W, Ning K, Zhang L, Marier SM, Liu Y, Chen Y, Xia F. Deep learning for time series forecasting: a survey. Int J Mach Learn Cybernet. 2025.
27. Shiri FM, Perumal T, Mustapha N, Mohamed R. A comprehensive overview and comparative analysis on deep learning models. J Artif Intell. 2024;6:301–60.
28. Zhang Y, Wang J. 1d cnn based network intrusion detection with normalization on imbalanced data. In: 2020 IEEE International Conference on Communications (ICC). IEEE, 2020:1–6.
29. Al-Selwi SM, Hassan MF, Abdulkadir SJ, Muneer A, Sumiea EH, Alqushaibi A, Ragab MG. Rnn-lstm: from applications to modeling techniques and beyond-systematic review. J King Saud Univ Comput Inf Sci. 2024;36(5): 102068.
30. He Y, Huang P, Hong W, Luo Q, Li L, Tsui K-L. In-depth insights into the application of recurrent neural networks (rnns) in traffic prediction: a comprehensive review. Algorithms. 2024;17(9):398.
31. Liu C-L, Hsaio W-H, Tu Y-C. Time series classification with multivariate convolutional neural network. IEEE Trans Industr Electron. 2019;66(6):4788–97.
32. Liu X, Cao C, Duan S. A low-power hardware architecture for real-time cnn computing. Sensors. 2023;23(4):2045.
33. Morais LBS, Aquila G, Faria VAD, Lima LMM, Lima JWM, Queiroz AR. Short-term load forecasting using neural networks and global climate models: an application to a large-scale electrical power system. Appl Energy. 2023;348: 121439.
34. Li H, Chen X. Detection of corona faults in switchgear by using 1d-cnn, lstm, and 1d-cnn-lstm methods. Sensors. 2023;23(5):2672.
35. Kiranyaz S, Avci O, Abdeljaber O, Ince T, Gabbouj M, Inman DJ. 1d convolutional neural networks and applications: a survey. Mech Syst Signal Process. 2021;151: 107398.
36. Cacciari I, Ranfagni A. Hands-on fundamentals of 1d convolutional neural networks—a tutorial for beginner users. Appl Sci. 2024;14(18):8500.
37. Hewamalage H, Bergmeir C, Bandara K. Recurrent neural networks for time series forecasting: current status and future directions. Int J Forecast. 2021;37(1):388–427.
38. Szostek K, Mazur D, Drałus G, Kusznier J. Analysis of the effectiveness of arima, sarima, and svr models in time series forecasting: a case study of wind farm energy production. Energies. 2024;17(19):4803.

39. Mahmoud A, Mohammed A. A survey on deep learning for time-series forecasting. In: Mahmoud A, Mohammed A, editors. Machine learning and big data analytics paradigms: analysis, applications and challenges. Studies in Big Data. vol. 77, pp. 365–392. Springer, 2020.
40. Rafi SH, Nahid-Al-Masood Deeba SR, Hossain E. A short-term load forecasting method using integrated cnn and lstm network. IEEE Access 2021;9.
41. Ige AO, Sibiya M. State-of-the-art in 1d convolutional neural networks: a survey. IEEE Access 2024;12.
42. Younesi A, Ansari M, Fazli M, Ejlali A, Shafique M, Henkel J. A comprehensive survey of convolutions in deep learning: applications, challenges, and future trends. IEEE Access. 2024;12.
43. Kim J, Kim H, Kim H, Lee D, Yoon S. A comprehensive survey of time series forecasting: architectural diversity and open challenges. arXiv preprint 2024.
44. Lim B, Zohren S. Time-series forecasting with deep learning: a survey. Philos Trans Roy Soc A Math Phys Eng Sci. 2021;379(2194):20200209.
45. Neumann O, Turowski M, Mikut R, Hagenmeyer V, Ludwig N. Using weather data in energy time series forecasting: the benefit of input data transformations. Energy Inf. 2023;6(1):44.
46. Mitchell AHG, Karoly DG. A comparison of methods for interpolating missing values in hourly precipitation time series. J Clim. 2004;17(17):3391–406.
47. Sánchez-Díaz MA, Fuente JM. Handling missing values in time series data. Int J Forecast. 2010;26(2):248–61.
48. Kumar S, Singh R. Islanding detection in microgrid using deep learning based on 1d cnn and cnn-lstm networks. ScienceDirect 2022.
49. Patel A, Sharma P. Short-term solar irradiance forecasting using cnn-1d, lstm, and cnn-lstm deep neural networks. ASME Digital Collection 2023.
50. Chakraborty S, Saha S. A comprehensive overview and comparative analysis on deep learning models. ResearchGate 2023.